



HAL
open science

A micro-hot-wire anemometry probe with elongated stubs for turbulent boundary layer measurements

Baptiste Baradel, Alain Giani, Fabien Méry, Philippe Combette, Olivier Léon

► **To cite this version:**

Baptiste Baradel, Alain Giani, Fabien Méry, Philippe Combette, Olivier Léon. A micro-hot-wire anemometry probe with elongated stubs for turbulent boundary layer measurements. 2024. hal-04648653

HAL Id: hal-04648653

<https://hal.science/hal-04648653>

Preprint submitted on 15 Jul 2024

HAL is a multi-disciplinary open access archive for the deposit and dissemination of scientific research documents, whether they are published or not. The documents may come from teaching and research institutions in France or abroad, or from public or private research centers.

L'archive ouverte pluridisciplinaire **HAL**, est destinée au dépôt et à la diffusion de documents scientifiques de niveau recherche, publiés ou non, émanant des établissements d'enseignement et de recherche français ou étrangers, des laboratoires publics ou privés.

A micro-hot-wire anemometry probe with elongated stubs for turbulent boundary layer measurements

Baptiste Baradel

Office National d'Études et de Recherches Aérospatiales

Alain Giani

IES, Université de Montpellier

Fabien Méry

Office National d'Études et de Recherches Aérospatiales

Philippe Combette

IES, Université de Montpellier

Olivier Léon

`olivier.leon@onera.fr`

Office National d'Études et de Recherches Aérospatiales

Research Article

Keywords:

Posted Date: March 20th, 2024

DOI: <https://doi.org/10.21203/rs.3.rs-4109150/v1>

License:  This work is licensed under a Creative Commons Attribution 4.0 International License.

[Read Full License](#)

Additional Declarations: No competing interests reported.

A micro-hot-wire anemometry probe with elongated stubs for turbulent boundary layer measurements

Baptiste Baradel^{1,2} · Alain Giani² · Fabien Méry¹ · Philippe Combette² · Olivier Léon^{1,†}

Pre-print version, March 17, 2024

Abstract The development of micro-hot-wire anemometry probes for turbulence studies requires mitigating spatial filtering, end-conduction effects and probe intrusivity. Keeping these factors in mind, this work analytically and experimentally investigates the relevance of a micro-hot-wire probe design featuring elongated stubs, inspired by Wollaston-wire probes but fabricated using modern micro-fabrication techniques. The resulting probes are shown to be relatively easy to manufacture and capable of providing satisfactory velocity measurements in a zero-pressure-gradient turbulent boundary layer at $Re_\tau \approx 1150$. Different probes were tested, all featuring a micro-wire length sufficiently small to alleviate spatial filtering of near-wall small-scale turbulent structures. The investigation focuses on assessing end-conduction effects and probe intrusivity, with the latter still observable close to the wall for such micro-probes.

1 Introduction

Hot-wire anemometry stands as a major measurement technique for investigating turbulence in free and wall-bounded flows (Bruun 1996; McKeon et al 2007; Smits 2022) as it offers continuous measurement of velocity fluctuations at a single point over a large range of frequencies. However, obtaining accurate results requires careful consideration of several important limitations. These include the spatial resolution of the probe, determined by the ratio of the wire's length to the characteristic length-scale of the flow under study. Additionally, internal heat-transfer effects can alter the probe spectral response, while the probe's cut-off frequency limits the resolvable time scales. Lastly, the intrusivity of the probe can introduce measurement errors.

Many of these challenges can be mitigated by reducing the dimensions of both the wire and the probe. This idea was particularly pursued by Willmarth and Sharma (1984) and Ligrani and Bradshaw (1987b) who used Wollaston wires to manufacture subminiature hot-wire probes. These wires consist of a thin silver-coated platinum(-rhodium) wire that is chemically etched to expose its core over a length ℓ , which defines the active part of the hot-wire probe. In their work, Ligrani and Bradshaw (1987a) and Ligrani and Bradshaw (1987b) reported the fabrication and use of such subminiature hot-wire probes with active sensing lengths ranging from $50\ \mu\text{m}$ to $300\ \mu\text{m}$, for wire diameters d as low as $0.625\ \mu\text{m}$. While measuring near-wall velocity fluctuations in a turbulent boundary layer (TBL), they notably emphasized the detrimental effects of thermal end-losses on the wire response for aspect ratios ℓ/d below 200 and significant spatial resolution issues with viscous-scaled wire lengths $\ell^+ = \ell U_\tau / \nu$ greater than 20. Here, U_τ refers to the mean friction velocity and ν denotes the fluid kinematic viscosity. The ratio of these two parameters defines the viscous length scale $l_v = \nu / U_\tau$. These criteria on ℓ and d are now regarded as standards for designing hot-wire probes employed in wall-bounded turbulence measurements. It highlights the importance of carefully selecting these geometrical parameters with respect to the viscous length scale of the flow of interest, with the condition $200d < \ell < 20l_v$ serving as a guideline for optimal design.

These bounds were reassessed by Hutchins et al (2009) at higher Reynolds numbers using different Wollaston hot-wire probes. While reaffirming the previous recommendations, they also suggested that the frequency response f_p of the hot-wire probe should be such that $f_p^+ = f_p \nu / U_\tau^2 \geq 1/3$ to effectively capture all relevant energetic scales. In the case of turbulent boundary layers commonly encountered in laboratory settings, this implies an anemometer capable of accurately resolving turbulence at frequencies typically exceeding 10 kHz. This frequency range may appear attainable with conventional hot-wire probes (i.e. $\ell \approx 1\ \text{mm}$

1. DMPE, ONERA, Université de Toulouse, France

2. IES, Université de Montpellier, France

† Corresponding author: olivier.leon@onera.fr

Distributed under [license CC-BY 4.0](https://creativecommons.org/licenses/by/4.0/)

and $d = 5\ \mu\text{m}$ typically) operated with a constant-temperature anemometry (CTA) system since it usually yields $-3\ \text{dB}$ cut-off frequencies greater than $50\ \text{kHz}$ based on an electronic square-wave test (SWT) response (Freythuth 1977). Yet, particular caution should be exercised when interpreting values obtained using electronic test responses since they do not directly account for unsteady heat conduction in the wire. This critical aspect has been extensively discussed in the works of Khoo et al (1999), Morris and Foss (2003), Li (2004) and Hutchins et al (2015) among others. These studies emphasize that the actual anemometer/probe cut-off frequency (from which deviation from a flat response is observed) can be about one order of magnitude lower than estimates obtained using the standard $-3\ \text{dB}$ drop-off from a SWT. This is the consequence of attenuation of heat waves along the wire. The attenuation magnitude ε is driven by the ratio ℓ/d among other factors (Hultmark et al 2011) and a characteristic attenuation time scale can be estimated by $\tau_w \approx \pi \ell^2 / (20 \alpha_w)$ for a cylindrical wire (Li 2004) with α_w the wire material thermal diffusivity. Hot-wires are generally designed to reduce the attenuation ε , but another strategy can be to design a wire with a characteristic time τ_w lower than the minimum turbulent time scale $t^+ = 3$ proposed by Hutchins et al (2009). This yields the criterion $\ell < 2\sqrt{\frac{15}{\pi \text{Pr}} \frac{\alpha_w}{\alpha_f} l_v}$, with Pr the Prandtl number of the fluid and α_f its thermal diffusivity. For a platinum wire used in air under normal conditions, this translates to $\ell < 6l_v$, a even more stringent criterion than the one previously obtained from spatial resolution considerations.

Overall, these recommendations point towards a more systematic use of small-scale hot-wire probes in turbulence studies, even at moderate Reynolds numbers. However, fabricating miniature hot-wire probes using Wollaston wires is a highly delicate task. Consequently, achieving functional probes smaller than those manufactured by Ligrani and Bradshaw (1987b) appears challenging without resorting to more recent micro-fabrication techniques. Early efforts were made by Löfdahl et al (1989) and Löfdahl et al (1992), leveraging MEMS (micro-electro-mechanical systems) fabrication technology. The designed probes provided adequate velocity measurements in a turbulent boundary layer, emphasizing the potential of the fabrication technique. However, these probes featured relatively large active elements, with the heating/sensing part having a minimum length of $300\ \mu\text{m}$ and a cross-section of $60\ \mu\text{m} \times 30\ \mu\text{m}$. Subsequently, Jiang et al (1994) micro-machined probes with a structural design closer to conventional hot-wires, using doped polysilicon. While achieving wire cross-section dimensions of $1\ \mu\text{m} \times 0.5\ \mu\text{m}$

and a length ℓ ranging from $10\ \mu\text{m}$ to $160\ \mu\text{m}$, these probes had relatively low wire aspect ratios, potentially making them susceptible to significant end-conduction effects. Additionally, temporal drifts were reported, and no clear demonstration of the probes for turbulence measurement was presented. Keeping the criterion $\ell/d > 200$ in mind, Löfdahl et al (2003) fabricated wall-mounted subminiature hot-wire sensors for shear-stress measurement. These sensors had minimum dimensions of $200\ \mu\text{m} \times 2\ \mu\text{m} \times 1\ \mu\text{m}$ and utilized aluminum for the wire material. While satisfactory results were obtained, to the best of our knowledge, their use was not expanded to more general turbulence measurement.

A major progress was made at Princeton University with the development of their Nanoscale Thermal Anemometry Probe (NSTAP). In its initial version presented by Bailey et al (2010) and adapted from Kunkel et al (2006), a $60\ \mu\text{m}$ long freestanding platinum wire with cross-section dimensions of $2\ \mu\text{m} \times 0.1\ \mu\text{m}$ was fabricated using chemical etching, focused ion beam milling and laser micromachining. This micro-wire was connected to the prongs by $60\ \mu\text{m}$ long and $15\ \mu\text{m}$ wide stubs to help minimize probe aerodynamic interference and thermal end-conduction effects. Although the probe proved effective for turbulence studies in a grid-generated turbulent flow, its application to wall-bounded turbulence measurement necessitated refinement to further decrease the aerodynamic interference induced by the tip of the support structure (Vallikivi 2014). A redesign of the probe and a different manufacturing approach using deep reactive ion etching (DRIE) were then proposed by Vallikivi et al (2011) and Vallikivi and Smits (2014). A smooth, streamlined V-shaped structure supporting the $60\ \mu\text{m}$ wire at its tip was obtained, and wire cross-section dimensions of $1\ \mu\text{m} \times 0.1\ \mu\text{m}$ were achieved. With this design, the $60\ \mu\text{m}$ long stubs extending the streamlined prongs were widened to $50\ \mu\text{m}$. This revisited probe was reported to significantly reduce intrusivity effects and provided satisfactory measurements in turbulent pipe flows and boundary layers (Vallikivi et al 2015; Samie et al 2018b). It can be noted, however, that to prevent any measurement drift the probe needs to undergo an annealing process, and possible residual blockage effects induced by the supporting structure may still be observable at high Reynolds numbers and close to the wall, as pointed out by Monkewitz (2021) and Smits (2022).

Variations of the NSTAP were designed to measure two velocity components (X-NSTAP, Fu et al (2019), Byers 2021), humidity (q-NSTAP, Fan et al (2015)) and for use in supersonic flows (Kokmanian et al 2019). While these applications involved variations in wire dimensions and the shape of stubs, the overall probe de-

sign remained similar. Lastly, a distinct probe featuring an even thinner freestanding platinum micro-wire with dimensions of $70\ \mu\text{m} \times 0.3\ \mu\text{m} \times 0.1\ \mu\text{m}$ was manufactured by Le-The et al (2021) at Twente University. This probe does not use stubs but instead relies on curved tapered prongs to support the micro-wire.

The current state-of-the-art in micro-fabricated hot-wire probes opens up promising avenues for in-depth studies of turbulence. Yet, the latest micro-probes have primarily focused on reducing intrusivity by profiling the prongs and questions about possible residual interference effects are left unanswered. This calls for exploration of alternative designs. Taking inspiration from the geometry of Wollaston-wire probes, the present work explores the fabrication and use of micro-fabricated hot-wire probes that rely on elongated stubs to mitigate probe intrusivity and wire end-conduction effects. The present micro-hot-wire (μHW) probes are shown to be manufacturable using simple fabrication steps, remarkably stable over time, and capable of providing adequate velocity measurements in a zero-pressure turbulent boundary layer.

2 Design and 1D model of a micro-hot-wire probe with thin elongated stubs

2.1 Design choices and dimensions

The geometry of the μHW probe selected for the present study is depicted in Figure 1. The design is intentionally simple, aiming to assess both the concept's relevance and the ease of probe fabrication. This probe comprises two prongs connected by an elongated micro-bridge, defining the stubs, which houses a ribbon-shaped micro-wire with a length ℓ at its center. Downstream of this micro-wire, a second non-conductive wire was added primarily to enhance the structural integrity of the bridge.

The chosen materials include silicon (Si) for the base structure, platinum (Pt) for the main electrically conducting layer, and nitride silicon (SiN_x) in between for electrical isolation. Detailed information about these different layers and the fabrication process is provided in Section 3.1. Importantly, the micro-wire is not designed as a freestanding Pt wire to simplify fabrication. Instead, it is structurally similar to the stubs, featuring a 200 nm-thick Pt layer deposited on a SiN_x layer of similar thickness. The total thickness of the micro-wire and the stubs is then $h \approx 400\ \text{nm}$. The implications of this two-layer design will be discussed in Section 2.2. Finally, the micro-wire width is set at $w = 1.5\ \mu\text{m}$ to facilitate fabrication using relatively straightforward pho-

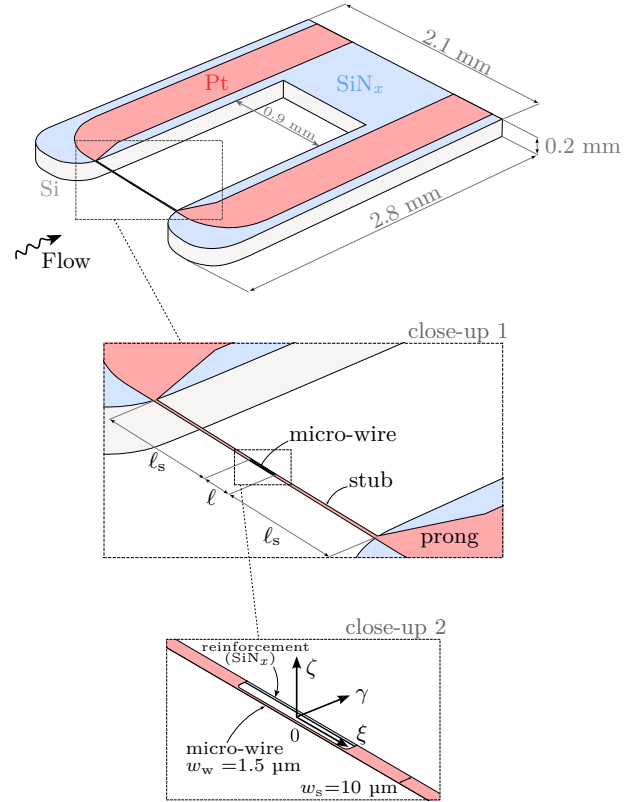


Fig. 1 Schematic and geometry of the micro-hot-wire probe.

tolithographic techniques while still providing suitably thin micro-wires for this work.

One objective of the present study is to identify the range of lengths ℓ that can be used to provide velocity measurements in a zero-pressure-gradient TBL without detrimental end-conduction effects. Indeed, the significance of end-conduction in this type of ribbon-shaped micro-wire with long stubs is largely unknown. To achieve this, spatial filtering effects must be avoided to eliminate this potential source of bias in the measurements. As detailed in Section 4, velocity measurements in the TBL are obtained at an axial location where the mean friction velocity U_τ is approximately $1\ \text{m s}^{-1}$, providing friction length scales l_ν in the order of $15\ \mu\text{m}$. Adhering to the previously discussed criteria, only micro-wire lengths lower than $300\ \mu\text{m}$ are then considered. Specifically, the chosen set of micro-wire lengths ℓ is $\{60, 80, 100, 150, 200\}\ \mu\text{m}$.

At this stage, it can be instructive to position this study with respect to two existing criteria used to characterize end-conduction attenuation effects. One approach is to rely on the ℓ/d criterion mentioned earlier, assuming an equivalent diameter d^* based on the cross-sectional area of the ribbon-shape micro-wires. This criterion would suggest that ℓ has to be larger than $174\ \mu\text{m}$. However, this is likely a conservative value be-

cause the micro-wire shape is not circular, and non-geometric, flow-related parameters also play a role in end-conduction effects. A potentially more suitable criterion has been proposed by [Hultmark et al \(2011\)](#) and refined by [Vallikivi \(2014\)](#). In the latter work, the criterion was extended to rectangular wire cross-sections and can be expressed as $\Lambda > [1.7, 2.5]$ for the NSTAP, with

$$\Lambda = \frac{\ell}{2w} \sqrt{\frac{2(h+w)}{h} \frac{k_f}{k_w} a \text{Nu}}, \quad (1)$$

where k_f and k_w refer to the thermal conductivity of the fluid (at film temperature) and wire, respectively, a to the wire resistance (overheat) ratio and Nu to the Nusselt number. As shown later in Section 4, the micro-wires in the present study cover a range of Λ values going from 2.07 to 6.95. However, it should be noted that this criterion was originally formulated for probes without stubs. Therefore, its applicability to the present probe geometry requires further investigation.

Regarding the stubs, their width was set to $10 \mu\text{m}$, approximately one order of magnitude greater than that of the micro-wire, to ensure reduced electrical resistance while still preventing significant aerodynamic interference. The implications of this design choice in terms of heat generation and transfer is discussed in Section 2.2, relying on an analytical model of the μHW probe. The total length of the micro-bridge was set to 0.9mm . This length was chosen based on our prior knowledge on the mechanical strength of similar elongated thermo-resistive wires manufactured for wall-stress measurements ([Weiss et al 2017](#)). It provides a separation between the prongs and the micro-wires ranging from 2ℓ to 7ℓ for the different micro-wire lengths considered.

2.2 A one-dimensional analytical model

With the design of the μHW probes defined, an analysis is first conducted to estimate their theoretical static and dynamic responses and to compare them with more conventional HW probes. Drawing upon the works of [Bruun \(1996\)](#), [Li \(2004\)](#) and [Li et al \(2004\)](#), the problem is approximated with a 1D model that takes into account the rectangular shape of the wire, the stubs, and the presence of a layer of SiN_x (which is an electrical insulator but a good thermal conductor) below the layer of Pt. In its general form, the 1D conservation equation of energy providing the unsteady temperature distribution along wire and stubs may be written

$$\tau \frac{\partial \theta}{\partial t} = \frac{\partial^2 \theta}{\partial \eta^2} - (p_\lambda - q_\lambda) \theta + Z_\lambda. \quad (2)$$

Using the subscript f to refer to the fluid conditions, θ is the local temperature ratio defined by

$$\theta(\eta) = \frac{T(\eta) - T_f}{T_f}, \quad (3)$$

where $T(\eta)$ is the local temperature. The coordinate ξ in wire direction and shown in Figure 1 has been made dimensionless using the micro-wire half-length, such that $\eta = 2\xi/\ell$. The coefficients of this differential equation are given by

$$\tau = \frac{\rho_b C_b \ell^2}{4 k_b} = \frac{\ell^2}{4 \alpha_b}, \quad (4a)$$

$$p_\lambda = \frac{P_\lambda \ell^2 \text{Nu}_\lambda k_f}{4 k_b A_\lambda w_\lambda}, \quad (4b)$$

$$q_\lambda = \frac{I^2 \ell^2 \alpha \chi_0}{4 k_b A_\lambda A_\lambda^{(\text{Pt})}}, \quad (4c)$$

$$Z_\lambda = \frac{I^2 \ell^2 \chi_f}{4 k_b A_\lambda A_\lambda^{(\text{Pt})} T_f}, \quad (4d)$$

where the subscript $\lambda \in \{\text{w}, \text{s}\}$ refers to the wire or stubs parameters, highlighting that the coefficients are actually piecewise functions of the coordinate η .

The time constant τ is obtained relying on a bulk, average density ρ_b , heat capacity C_b and heat conductivity k_b of the two layers of Pt and SiN_x lumped together. This approximation neglects heat transfers between the two layers, but this is reasonable at first order given the thinness of the layers and their comparable material properties. The associated cross-sectional Biot numbers are in the order of 1×10^{-4} , thus sufficiently small to consider uniform temperature in wire cross-sections at all times. This characteristic time τ should be seen as indicative of the characteristic attenuation time scale of the wire and is thus similar to τ_w previously discussed, with α_b the bulk thermal diffusivity.

The dimensionless parameter p_λ is defined using the cross-sectional perimeter $P_\lambda = 2(w_\lambda + h)$, the cross-sectional area $A_\lambda = w_\lambda h$ and the Nusselt number. Considering the shape of the wire, the Nusselt number is estimated using the relation for laminar flow over two sides of a flat plate, writing

$$\text{Nu}_\lambda = 0.664 \text{Re}_\lambda^{0.5} \text{Pr}^{0.33} \quad (5)$$

with the Reynolds number $\text{Re}_\lambda = U w_\lambda / \nu$ (in the order of unity) and the Prandtl number $\text{Pr} \approx 0.71$. The characteristic convection length is taken as the local width w_λ . Particularly relevant for the wire itself, the parameter p_w can be regarded as equivalent to a Biot number Bi_w based on the length $L_{cw} = (\ell/2)^2 P_w / A_w$, such that $p_w = \text{Bi}_w = h_{cw} L_{cw} / k_b$ where $h_{cw} = \text{Nu}_w k_f / w_w$ refers to the convective heat transfer coefficient on the wire. This Biot number expresses the ratio of heat convection

on the wire to internal heat conduction, which is generally desired to be as large as possible for HW probes to reduce end-conduction effects. It may be noted that it is related to Λ defined by Vallikivi (2014) (and similarly to Γ defined by Hultmark et al (2011)) since $\Lambda = \sqrt{a\text{Bi}_w}$ with a the wire resistance overhear ratio.

Finally, the two dimensionless terms q_λ and Z_λ account for heat generation by Joule effect and are defined using the current intensity I , the cross-sectional area of the Pt layer $A_\lambda^{(\text{Pt})}$ (since only the platinum layer is electrically conductive), the temperature coefficient of resistance α (TCR), the platinum resistivity at $T_0 = 0^\circ\text{C}$ noted χ_0 and the platinum resistivity at fluid temperature T_f noted χ_f . The evolution law of the resistivity is assumed to be linear such that

$$\chi(T) = \chi_0 (1 + \alpha(T - T_0)). \quad (6)$$

The term q_λ can be seen as a ratio of heat generation to heat conduction. In the case of a wire without stubs, it appears in the definition of Betchov's cold length $\ell_c = \ell/(2Y_w)$ with the dimensionless parameter $Y_w = \sqrt{|p_w - q_w|}$ (Bruun 1996). This parameter is referred to by Li et al (2004) and McKeon et al (2007) as a Biot number because of the presence of p_w , but it also integrates heat generation effects through q_w . The important point is that Y_w can serve as a general parameter to quantify end-conduction effects since large values imply small wire cold lengths ℓ_c . As detailed by Bruun (1996), the parameter Y_w (noted K_1 in this reference) can be expressed using the (inverse) overhear resistance ratio $a_\infty = R_{wa}/R_{w\infty}$ with R_{wa} as the wire resistance at ambient temperature and $R_{w\infty}$ as the one in the (hypothetical) case where there are no end-conduction losses, such that $Y_w = \sqrt{a_\infty p_w} = \sqrt{a_\infty \text{Bi}_w}$. One can clearly see that Y_w is very similar to the parameter Λ , except for the different definitions of the resistance ratios a and a_∞ . Y_w will be referred to as an extended Biot number in the present work.

2.3 Steady-state solution

In steady condition, equation (2) writes

$$\frac{d^2\bar{\theta}}{d\eta^2} - (\bar{p}_\lambda - \bar{q}_\lambda)\bar{\theta} + \bar{Z}_\lambda = 0, \quad (7)$$

with overbars denoting static variables. This ODE can be solved analytically (using symbolic computing in the case with stubs) to evaluate the static temperature distribution \bar{T} in the wire and the stubs. It is assumed that $\bar{\theta} = 0$ at the prongs only. Furthermore, at the junctions between wire and stubs ($\eta = \pm 1$), continuity of $\bar{\theta}$ and heat flux conservation are enforced.

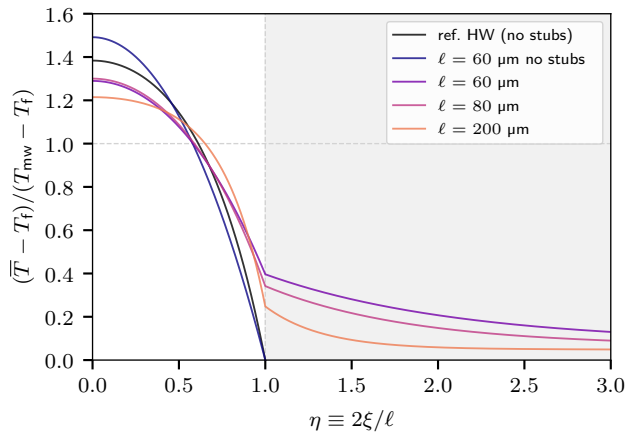


Fig. 2 Dimensionless static temperature distribution for different hot-wire configurations. The gray area highlights the region where a stub is present, if any. Operating conditions are provided in Table 1. T_{mw} refers to the mean temperature of the wire.

Solutions obtained for HW probes without and with stubs are shown in Figure 2. Here, a mean flow velocity $U = 10 \text{ ms}^{-1}$ is selected to be similar to that observed at the location of maximum fluctuation in the TBL studied in Section 5, and the intensity I in each wire is selected to provide a mean temperature T_{mw} of the (micro-)wire itself of about 220°C . The first probe is a conventional tungsten HW probe without stubs, with a diameter of $5 \mu\text{m}$ and a length of 1.25 mm , thus having a ratio $\ell/d = 250$. Its dimensionless temperature distribution is relatively similar to that obtained considering a μHW probe of length $\ell = 60 \mu\text{m}$ without stubs, which is consistent with the work of Bailey et al (2010) on the NSTAP. However, a major difference between these two probes is found in the ratio of heat conducted to the prongs to total heat generated by Joule effect, noted σ_w (Freytmuth 1979). The values are given in Table 1, showing that 54% of the heat is lost to the prongs in the case of a $60 \mu\text{m}$ long μHW without stubs while it is 22% for the reference HW probe for this flow condition. This is the result of a significantly lower extended Biot number Y_w in the case of the micro-probe, suggesting potentially greater attenuation of heat waves compared to the reference probe. However, as demonstrated later, this attenuation manifests at much higher frequencies due to the reduced characteristic time of the micro-wire.

The addition of thin, elongated stubs significantly modifies this static temperature distribution. This is illustrated by considering three μHW probes with wire lengths of $60 \mu\text{m}$, $80 \mu\text{m}$ and $200 \mu\text{m}$. As depicted in Figure 2, more uniform temperature distributions along the micro-wires are achieved. While part of the generated heat is conducted to the stubs, where non-linear

	Re_w	Nu_w	A	Y_w	σ_w
ref. HW (no stubs)	3.32	1.26	5.09	2.49	0.22
$\ell = 60 \mu\text{m}$ no stubs	1.0	0.59	2.08	0.59	0.54
$\ell = 60 \mu\text{m}$	1.0	0.59	2.08	0.92	0.42
$\ell = 80 \mu\text{m}$	1.0	0.59	2.77	1.39	0.32
$\ell = 200 \mu\text{m}$	1.0	0.59	6.95	3.98	0.12

Table 1 Dimensionless parameters for the modeled HWs and considering a flow velocity $U = 10 \text{ m s}^{-1}$ at a static temperature $T_f = 20^\circ\text{C}$. The reference HW is a classical 1.25 mm long, 5 μm tungsten wire operated at an overheat ratio of 0.8. The modeled μHWs , with their geometry defined in Section 2.1, are operated without or with elongated stubs at a wire overheat ratio of 0.66.

temperature profiles are then observed, this heat loss is reduced compared to the case without stubs. This is quantified in Table 1, showing for instance that the inclusion of stubs in the 60 μm long μHW increases Y_w from 0.59 to 0.92 and decreases σ_w from 54% to 42%. By construction, this improvement is not captured by the A parameter since the effects of stubs on the boundary conditions are discarded in its derivation. Increasing the micro-wire length further increases the extended Biot number and decreases the percentage of heat lost to the stubs, suggesting further improvement in mitigating heat-waves attenuation.

2.4 Dynamic response and wire attenuation

To support these results and gain a better understanding of the impact of such elongated stubs on the dynamic response of micro-wires, a simplified analytic approach is considered. Using equations (2) and (7), the equation governing small temperature fluctuations in the micro-wire is expressed as

$$\tau \frac{\partial \theta'}{\partial t} = \frac{\partial^2 \theta'}{\partial \eta^2} - (p'_w - q'_w) \bar{\theta} - (\bar{p}_w - \bar{q}_w) \theta' + Z'_w, \quad (8)$$

where the primes indicate fluctuations. This equation can be reorganized to collect the terms related to velocity and intensity fluctuations, denoted as u' and i' , respectively, and contained in p'_w , q'_w and Z'_w . The reader is referred to the work of Li (2004) for details on the approach followed to assess the wire response in terms of magnitude of the transfer function $D(\omega) = \hat{i}'(j\omega)/\hat{u}'(j\omega)$ where $j\omega$ refers to the complex angular frequency and the hat to Laplace transformed variables. The normalized transfer function amplitude is expected to provide relevant quantitative results for comparing attenuation effects in different wires.

However, it is important to note that this analysis has limitations and will not perfectly model the true, experimental wire responses. Three key simplifications are emphasized. Firstly, resistance fluctuations

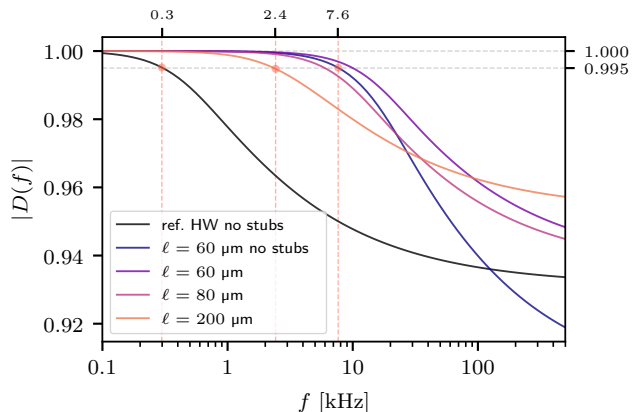


Fig. 3 Dynamic response of the different hot-wires considered in Figure 2 and Table 1 in terms of magnitude of the complex transfer function $D = \hat{i}'/\hat{u}'$ for a range of the perturbation frequency f . Amplitudes are normalized using values at $f = 100 \text{ Hz}$.

of the stubs are ignored. It is assumed that overall resistance fluctuations are mainly influenced by those of the micro-wire, owing to the significant difference of thermal inertia and heat exchange with the flow between the two elements. This implies that the effect of the stubs on the dynamical response of the wires is solely captured through a modification of the static temperature distribution. Secondly, the analysis considers only uniform velocity perturbations along the micro-wire, despite the presence of various transverse turbulent length scales interacting with it. Lastly, perfect wire resistance compensation at all times is assumed, neglecting coupling with the CTA system. While this aspect is beyond the scope of this analysis, it may be explored further following the work of Li (2004) and Samie et al (2018a) for instance.

Figure 3 displays the magnitude of the transfer function for the different hot-wires considered in Figure 2. Similarly to Li (2004), the reference 1.25 mm long HW begins to exhibit attenuation at a few hundred Hertz. In contrast, a μHW designed without stubs (thus relatively similar to a NSTAP) significantly increases this cut-off frequency to around 8 kHz but also displays a larger and steeper attenuation beyond this threshold. This substantial high-frequency attenuation may not pose a severe limitation depending on the specific frequency content of the flow under consideration, as demonstrated for example by NSTAP measurements reported in the work of Samie et al (2018b). More importantly for the present study, the addition of stubs to this micro-wire appears to mitigate this high-frequency attenuation, approximately halving it and consequently improving the micro-wire cut-off frequency. Moreover, increasing the micro-wire length further reduces the attenuation,

but at the cost of a reduction in the micro-wire cut-off frequency. These results suggest for instance that spectral differences may be experimentally observed between the 60 μm and 200 μm μHW probes for frequencies around 10 kHz. This point is further discussed in Section 5, where no such differences are reported.

This analysis suggests that incorporating thin, elongated stubs, as proposed in Section 2.1, should overall improve the spectral response of a micro-wire. However, an experimental validation is necessary due to the limitations of this analytical approach. This is addressed in the rest of this work. Section 3 provides details on the manufacturing process of such μHW probes and analyses their steady electrical and aerodynamic responses. These probes are then tested to measure near-wall velocity fluctuations in a turbulent boundary layer: Section 4 provides a description of the experimental setup and the actual performance of the μHW probes are finally discussed in Section 5.

3 Fabrication and characterization of the probe

3.1 Manufacturing process

The fabrication steps for the μHW probes involve several key processes. The primary structural material is silicon, a semiconductor largely used in microtechnology. Starting with a 4 inch 200 μm -thick double-side polished Si wafer, 200 nm-thick layers of silicon nitride (SiN_x) are formed on both sides through Low-Pressure Chemical Vapor Deposition (LPCVD). This deposition method yields flat and robust electrically insulating layers with low residual tensile stresses and ensures consistent repeatability in fabrication (Temple-Boyer et al 1998).

Subsequently, a single 200 nm-thick layer of platinum is added using Electron Beam Physical Vapor Deposition (EBPVD), providing thermo-resistive parameters closely matching those of bulk Pt. Platinum is chosen as the conductive material for the micro-wires due to its durability and stability. Importantly, a very thin tantalum oxide (Ta_xO_y) adhesive layer is added before Pt deposition (Johnson et al 1990). This adhesive layer plays a crucial role in ensuring the long-term stability of the thermo-resistive properties of the wires discussed in Section 3.2.

Once this stack of materials is obtained, standard semi-conductor fabrication techniques are used to produce the μHW s. The different steps are summarized in Figure 4. Before each step, the samples undergo a careful cleaning process in ultrasound baths filled with acetone and ethanol, followed by rinsing with de-ionized water and dehydration. Each layer of Pt and SiN_x

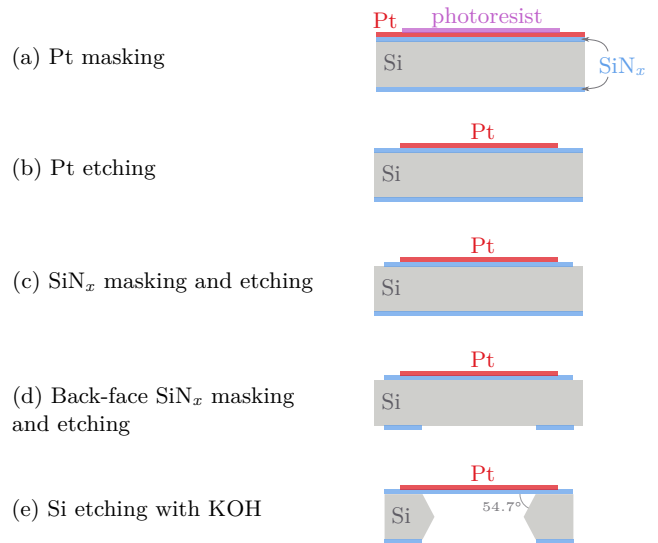


Fig. 4 Schematic of the manufacturing steps of the μHW probes (cross-sectional view containing the micro-wire).

is then sequentially patterned using photo-lithography and etched by Reactive Ion Etching (RIE) (Figures 4(a-d)). The final step aims at shaping the Si substrate, without the requirement to produce streamlined sensors as explained in Section 2.1. An alkaline solution of potassium hydroxide (KOH) is thus used to etch the silicon and free the elongated bridge and the micro-wire. Importantly, this solution etches the silicon substrate following its crystal planes. Using a $\langle 100 \rangle$ orientation Si wafer, etching occurs at an angle of 54.7° from the horizontal axis (Figure 4(e)). Therefore, particular attention has to be given to the design of the photo-lithographic masks to account for this. Finally, the samples are rinsed in a deionized water solution and are briefly immersed in acetone and isopropanol to remove potential residues.

An example of a μHW probe is presented in Figure 5(a) with a detailed focus on the micro-wire itself shown in Figure 5(b). The μHW probe is mounted onto a custom Printed Circuit Board (PCB) connector, specifically designed to fit into standard HW probe supports. This connector eliminates the need for conductive glue, which could introduce additional contact resistances between the sensor and its support. In this design, the connection is done using aluminum bonding wires that were found to be very robust across various flow conditions.

3.2 Electrical properties

Adjusting the operating overheat ratio of each μHW probe requires knowledge of their thermo-resistive pa-

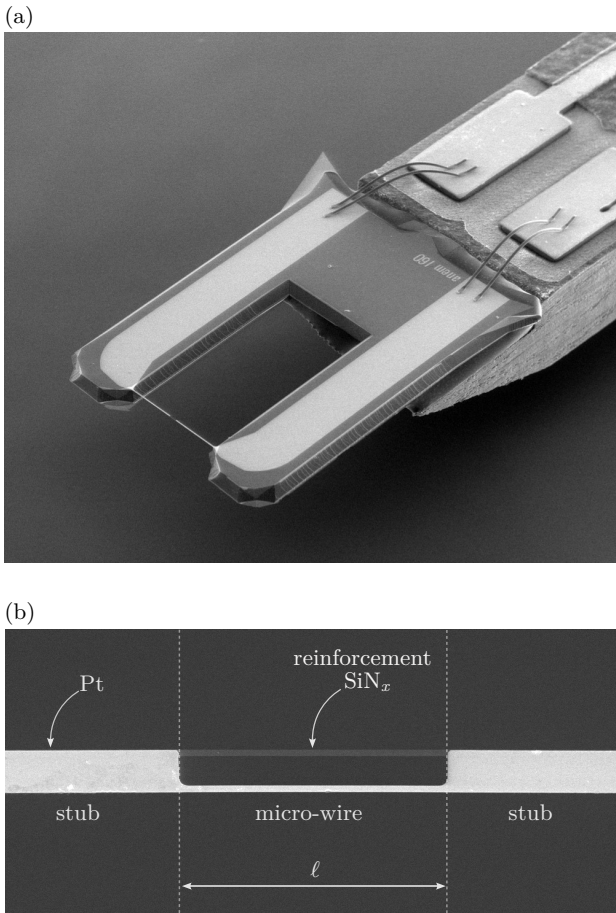


Fig. 5 (a) Scanning Electron Microscopy (SEM) image of a μHW probe with $\ell = 60 \mu\text{m}$ mounted on a custom PCB connector; (b) Close-up of the micro-wire.

rameters, namely R_0 , which is the resistance at 0°C , and α , the temperature coefficient of resistance.

These parameters are estimated for each μHW probe by placing them in a calibration oven and measuring the total probe resistance $R(T)$ across a temperature range using a constant current of 0.1 mA . A linear-regression then provides estimates of R_0 and α . These parameters apply to the entire μHW probe rather than the micro-wire alone. The value of R_0 thus depends on the lengths of both the stubs and the micro-wire. For instance, at an ambient temperature of 20°C , the total resistance of a μHW probe with $\ell = 60 \mu\text{m}$ is in the order of 100Ω , while it is approximately 160Ω for $\ell = 200 \mu\text{m}$. The resistances of the micro-wires themselves can be estimated knowing the geometry of the probes and the resistivity of Pt, resulting in values of approximately 35Ω and 110Ω at ambient temperature, respectively.

The TCR α is solely determined by the wire material and remains constant for every μHW probe, regardless of the micro-wire length. The values obtained

are in the order of $0.0036^\circ\text{C}^{-1}$. These values are near that of bulk platinum $\alpha_{\text{Pt}} = 0.0039^\circ\text{C}^{-1}$, which is beneficial since large TCR values enhance the probe sensitivity. For comparison, the Pt-based micro-probes fabricated at Princeton University and at Twente University have significantly lower TCR values, of approximately $0.0021^\circ\text{C}^{-1}$ (Vallikivi and Smits 2014; Le-The et al 2021).

The stability of the μHW probes was studied to evaluate the magnitude of temporal drift of resistance during operation. Tests were performed by setting a newly fabricated μHW probe at a temperature of 200°C for several days. Its resistance was continuously monitored and the largest amplitude variation observed over 17 days was about $\pm 1.1\%$ of the mean value. These minute variations are however likely the result of minor changes in the oven temperature rather than changes in the thermo-resistive parameters of the probe. This excellent stability was finally also observed during operation in wind-tunnels, confirming that no prior annealing of the probe is necessary, an aging process that is sometimes required for HW probes (Vallikivi and Smits 2014).

3.3 Operation and aerodynamic calibration

The μHW probes were operated at constant temperature to perform velocity measurements. This was achieved using a commercial CTA module from Dantec Dynamics (90C10) operated with a 1:1 bridge and an external resistor to set the resistance overheat ratio at an approximate value of 0.7.

The static response of the μHW probes was studied using a jet calibration unit regulated in velocity. The mean CTA output voltage E is given as a function of the mean flow velocity U in Figure 6 for a μHW probe with $\ell = 60 \mu\text{m}$. An excellent fit with a unit correlation coefficient is observed using the classical King's law expressed as $E^2 = a + bU^n$ where a , b , and n are the calibration parameters. This excellent fit, even observed for low velocities, supports the use of such a law despite the non-cylindrical shape of the micro-wires, which is consistent with the work of Vallikivi (2014) on the NSTAP for example. Similar fit results were obtained with the others μHW probes.

For wind tunnel measurements, each μHW calibration was performed with an assumed uncertainty on the mean flow velocity measured by a Pitot tube of $\pm 1\%$. The uncertainties and covariances of the calibration parameters were assessed based on this estimate, resulting in uncertainty intervals provided in Figure 6.

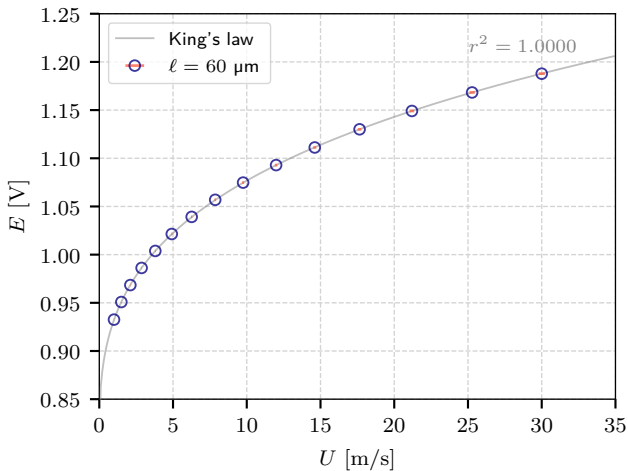


Fig. 6 Calibration results for a μ HW probe with $\ell = 60 \mu\text{m}$ and fitted with King's law. Uncertainties on velocity measurements of $\pm 1\%$ are indicated using red error bars. Resulting uncertainties on the parameters a , b and n are $\pm 0.23\%$, $\pm 0.61\%$, $\pm 0.37\%$, respectively.

3.4 Square wave test response

As mentioned in Section 1, the SWT does not fully capture the frequency response of a HWA system. It is primarily used here to demonstrate the stability of the HWA system operating with a μ HW probe in CTA mode and to compare responses with conventional HW probes.

Figure 7(a) presents examples of SWT responses obtained using both a reference 1.25 mm HW and a 80 μm μ HW in a uniform flow at 25 m s^{-1} . For these measurements, the tuning parameters of the CTA module were set to their minimum values, allowing a comparison of the responses of the two HWA systems with similar configurations. Characteristic time responses are provided, corresponding to SWT cut-off frequencies of approximately 51 kHz for the system with the reference HW probe and 118 kHz for the one with the μ HW probe.

Tuning the CTA module can reduce this characteristic time. An optimized response for the HWA system operating the μ HW probe is illustrated in Figure 7 for mean flow velocities of 10 m s^{-1} and 25 m s^{-1} , with the former corresponding to the velocity measured at the location of maximum velocity fluctuation in Section 5. In both cases, stable operation is observed, with a SWT cut-off frequency of approximately 145 kHz and a slightly under-damped temporal response (Bruun 1996; Hutchins et al 2015).

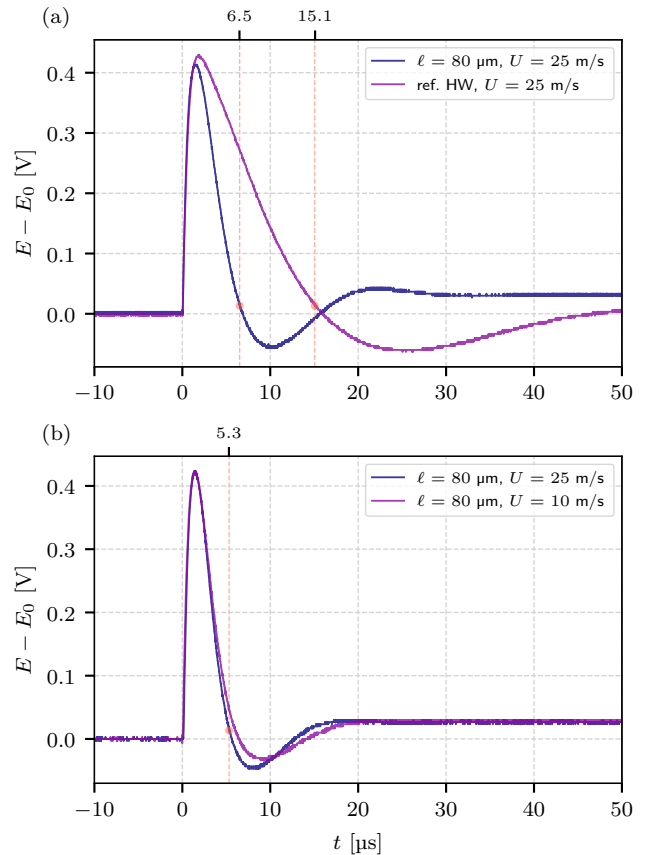


Fig. 7 SWT responses for (a) a reference 1.25 mm HW probe and an 80 μm μ HW placed in a uniform flow at 25 m s^{-1} with minimal tuning of the CTA system, and (b) the same μ HW probe but with improved CTA tuning, tested at two flow velocities. The vertical red dashed line marks the temporal delay τ_3 for which 3% of the maximum amplitude is reached. This value is commonly used to estimate the SWT cut-off frequency as $1/(1.3\tau_3)$ (Freyth 1977).

3.5 Angular sensitivity

The angular configuration of a HW probe can significantly impact measurements due to disturbances induced by elements like the prongs and the stem (Comte-Bellot et al 1971). In addition, the present micro-wire is not circular but has a ribbon shape, and the current probes have to be slightly inclined to perform near-wall velocity measurements. Therefore, a sensitivity analysis to pitch angle ϕ was conducted to gain further insight into the performance of the μ HW probes.

The pitch sensitivity of a 60 μm μ HW probe is displayed in Figure 8 alongside measurements obtained with a NSTAP. While both probes exhibit relatively similar trends, slight differences can nonetheless be emphasized. Firstly, for negative pitch angles, the velocities measured by the μ HW probe tend to be underestimated, whereas the NSTAP yields slightly overesti-

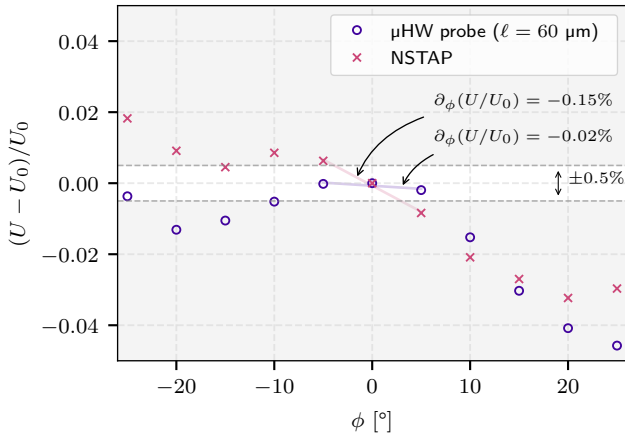


Fig. 8 Sensitivity to pitch angle ϕ of a μ HW probe ($\ell = 60 \mu\text{m}$) and a NSTAP. U is the mean velocity measured by the probe and U_0 is the one measured at $\phi = 0^\circ$.

ated values. Secondly, the derivative $\partial(U/U_0)/\partial\phi$ for the μ HW probe is close to zero around $\phi = 0^\circ$, indicating minimal sensitivity of the probe to pitch angle within the range of $\pm 5^\circ$. This result could be attributed to the use of elongated stubs, which are expected to reduce the influence of the prongs on the flow interacting with the micro-wire.

For velocity measurements in a TBL, it is then recommended to operate the μ HW probes with a pitch angle in the range of $\pm 5^\circ$ to minimize probe disturbance effects. However, this analysis was conducted in a free flow, and additional disturbances should be expected when the probe is placed close to a wall as highlighted in Section 5.

4 Experimental study in a turbulent boundary layer

The performance of μ HW probes with different micro-wire lengths was experimentally assessed by measuring velocity profiles in a zero-pressure-gradient turbulent boundary layer. This section details the experimental setup used (Section 4.1), some characteristics of the TBL (Section 4.2), the way TBL parameters and uncertainties are evaluated (Section 4.3) and the different types of probes that were operated (Section 4.4).

4.1 Experimental setup

The experiments were conducted in an open return wind tunnel with a working section measuring $2.5 \text{ m} \times 0.4 \text{ m} \times 0.3 \text{ m}$, where a 1.8 m aluminum flat plate featuring an elliptical leading edge was mounted. The boundary layer developing on this plate was triggered using a

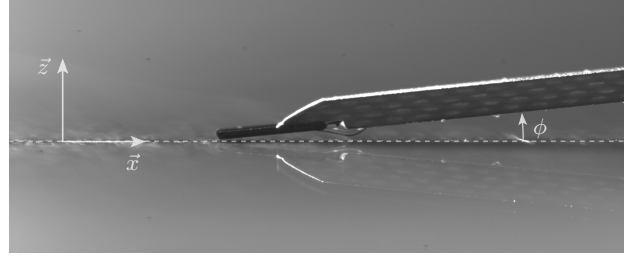


Fig. 9 Photograph of a μ HW probe positioned on a flat plate with an absolute pitch angle $|\phi| = 5.3^\circ$.

0.3 mm thick zig-zag tape positioned 10 cm away from the leading edge.

Velocity measurements with the different HW probes considered in this work were obtained at an axial location 1.3 m from the leading edge. A Pitot tube was installed at this location, in the uniform freestream region, serving as a reference for in-situ velocity calibration of the HW probes.

Positioning of all the HW probes relative to the wall was achieved using a 5 Mpx camera equipped with a 180 mm macro lens. This allowed to adjust the vertical location of the probes with a visual accuracy of about $50 \mu\text{m}$, but it also provided a way to evaluate the pitch angle, as illustrated in Figure 9 where $|\phi| = 5.3^\circ$. As also shown in this figure, the μ HW probes were used upside-down, thus with an actual negative pitch angle. This orientation of the probe allows to position the micro-wire closer to wall, without being constrained by the thickness of the Si substrate. However, this positioning approach does not provide a sufficiently accurate estimate of the distance of the wire from the wall, which is an important variable in the identification process of the TBL parameters (Örlü et al 2010). The exact wall location is then later corrected during post-processing of the velocity profiles as detailed in Section 4.3. Finally, the HW probes are traversed within the TBL using a precision linear stage (Newport UTS 150-PP), having a displacement accuracy of $\pm 1.7 \mu\text{m}$.

All the HW probes were controlled with the same CTA module (90C10, Dantec Dynamics). The μ HW probes and the NSTAP were operated as detailed in Section 3.3 whereas the reference 1.25 mm HW probe was operated using a 1:20 bridge. The CTA module output signal was directly acquired using a 24-bit acquisition card (NI-9239) at a frequency of 50 kHz. For each measurement point in the TBL, the CTA signal was acquired over a duration T_{ac} of 30 s, yielding more than 40 000 boundary layer turnover times δ/U_∞ , which is considered sufficient to provide converged TBL statistics (Hutchins et al 2009). Concurrently, freestream measurements obtained from the Pitot tube and a thermocouple were acquired to discard measurements for

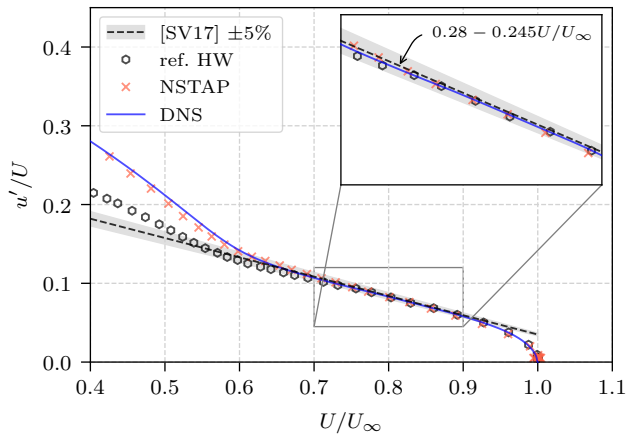


Fig. 10 Diagnostic plot of velocity measurements obtained with a reference 1.25 mm HW and with a NSTAP. The inset highlights the comparison with the linear relation proposed by [Sanmiguel Vila et al \(2017\)](#) for a well-behaved ZPG TBL and with DNS results provided by [Schlatter and Örlü \(2010\)](#) for a TBL profile at $\delta^+ = 1145$.

which external velocity and temperature varied by more than $\pm 0.5\%$ during one complete traverse.

4.2 Details on the TBL

The wind tunnel was operated at a freestream velocity $U_\infty = 25 \text{ m s}^{-1}$ with its ceiling adjusted to yield a zero-pressure-gradient (ZPG) TBL. At the axial location where HW measurements were performed, the resulting mean friction velocity U_τ is in the order of 1.0 m s^{-1} and the TBL thickness δ_{99} is approximately 18 mm. Under normal atmospheric conditions, with $T_{\text{atm}} = 20^\circ\text{C}$, the friction Reynolds number is then $\text{Re}_\tau = \delta_{99}^+ \approx 1150$. Significant energetic content is observed up to $f_{\text{max}} \approx 20 \text{ kHz}$ and $f_{\text{max}}^+ \approx 0.3$, a value in agreement with the upper bound proposed by [Hutchins et al \(2009\)](#). This frequency is below the Nyquist frequency of the acquisition system, preventing aliasing.

To better assess the state of the present TBL, a simple approach is to rely on the diagnostic plot proposed by [Sanmiguel Vila et al \(2017\)](#), which does not require any estimate of the wall position or friction velocity. In Figure 10, the ratio u'/U of (sample) velocity standard deviation to mean velocity is displayed as a function of the normalized mean velocity U/U_∞ for measurements obtained using a reference 1.25 mm HW probe and using a NSTAP provided by Princeton University. These results can be compared to the linear empirical relation proposed by [Sanmiguel Vila et al \(2017\)](#) in the outer region of the TBL (such that $0.7 < U/U_\infty < 0.9$), and expressed as

$$\frac{u'}{U} = \gamma - \beta \frac{U}{U_\infty} \quad (9)$$

with $\gamma = 0.28$ and $\beta = 0.245$ for “well-behaved” ZPG TBLs. A satisfactory agreement is obtained in this region of the TBL for both sets of measurements, indicating a relative canonical state. Differences between the reference HW and the NSTAP measurements are however observed in regions of the TBL closer to the wall, for $U/U_\infty < 0.7$. This discrepancy reflects the effect of spatial filtering of the small eddies by the reference 1.25 mm HW. This is particularly emphasized by comparing the measurements with DNS results provided by [Schlatter and Örlü \(2010\)](#) for a ZPG TBL at $\delta^+ = 1145$, showing a satisfactory match with NSTAP data.

4.3 Measurement uncertainties and TBL parameters estimation

The main source of uncertainty in the HW velocity measurements was estimated to originate from the HW calibration. Other sources of uncertainty such as statistical estimation, atmospheric variations and voltage reading were found to be comparatively negligible by at least one order of magnitude. Calibration uncertainties were propagated to mean and velocity variance estimates obtained from HW measurements using a Monte Carlo approach that relies on the uncertainty covariance matrix of the calibration parameters, as detailed for example by [Rezaeiravesh et al \(2018\)](#).

TBL parameters were then evaluated by fitting a composite analytical profile proposed by [Chauhan et al \(2007\)](#) to the mean velocity measurements with uncertainty, thus providing estimates for the mean friction velocity U_τ , the wake parameter II and the (theoretical) boundary layer thickness δ . Furthermore, given the relative canonical state of the present ZPG TBL, the minimized objective function was augmented by an additional loss on the wall location z_0 , promoting a location of the peak of velocity variance near $(z - z_0)^+ = 15$. The value of the von Kármán constant is here assumed to be 0.384 following [Nagib and Chauhan \(2008\)](#).

As a result, uncertainties on the estimated TBL parameters were also obtained, with a typical interval of $\pm 0.5\%$ for the mean friction velocity U_τ . However, this approach assumes that no bias is present in the measurements and that the chosen model is perfect. As discussed in Section 5, the present near-wall HW measurements are most likely biased due to intrusivity effects. Given the definite influence of near-wall mean velocity on the estimated parameters, the initial data points are discarded, and for this indirect approach, it was considered more reasonable to assume an actual uncertainty on U_τ of $\pm 1\%$. This uncertainty on U_τ was finally algebraically propagated to estimates of inner-scaled quan-

Probe	ℓ (μm)	ℓ^+	ℓ/w	ℓ/t	Λ	Y_w	σ_w
ref. HW	1250	81.34	250	250	5.09	2.49	0.22
μHW	60	3.90	40	150	2.07	0.92	0.42
μHW	80	5.21	53	200	2.77	1.39	0.32
μHW	100	6.51	67	250	3.45	1.85	0.26
μHW	150	9.76	100	375	5.19	2.93	0.16
μHW	200	13.01	133	500	6.95	3.98	0.12
NSTAP	60	3.90	30	600	2.01	1.17	0.52

Table 2 Characteristics of the different probes used for TBL measurements: length of the hot-wire element ℓ , ratios to other characteristic lengths (ℓ^+ , ℓ/w and ℓ/t), and estimated parameters for quantification of end-conduction effects for a mean flow velocity of 10 m s^{-1} (Λ , Y_w and σ_w). The last two parameters are estimated relying on the analytical model described in Section 2.2.

tities such as U^+ and $(u'^2)^+$. It is emphasized that, by definition, the uncertainties evaluated for these quantities cannot account for potential sources of biases.

4.4 Tested HW probes

The five μHW probes selected in Section 2.1 were manufactured and used for TBL measurements. Dimensional characteristics are summarized in Table 2 and can be compared with those of the reference HW probe and the NSTAP. Notably, only the reference probe presents a viscous-scaled wire length ℓ^+ greater than 13, thus yielding spatially-filtered results, as already illustrated in Figure 10.

Table 2 also presents estimates for three parameters defined in Section 2.2, aiming to evaluate the importance of end-conduction effects. Values of the Λ parameter range from 2 to 7 for the μHW probes; however, these values are provided for reference only, as this parameter is not specifically tailored to account for the presence of elongated stubs, as discussed in Section 2.3. More relevant for this study, the values of the extended Biot number Y_w range from 0.9 to 4, while the percentage of heat conducted to the stubs ranges from 42% to 12%, respectively.

5 Results and discussion

5.1 Velocity statistics

The diagnostic plot in Figure 11 shows velocity measurements obtained with the HW probes listed in Table 2. The various μHW probes tested exhibit consistent

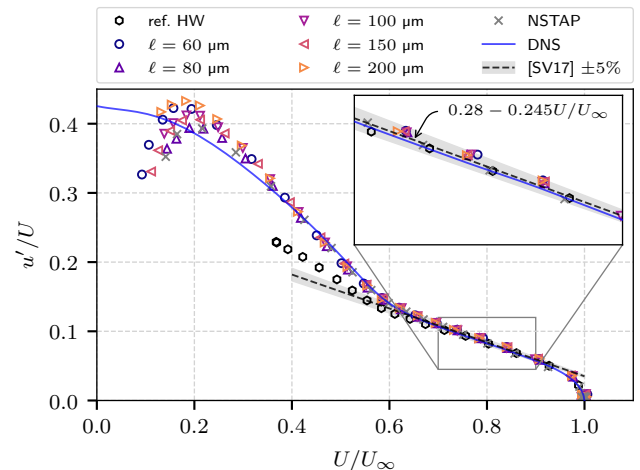


Fig. 11 Diagnostic plot of velocity measurements obtained using a reference HW probe, μHW probes with different micro-wire lengths ℓ and a NSTAP. The same DNS dataset as in Figure 10 is used for comparison.

profiles, aligning well with NSTAP results and DNS data. Although minor differences may be observed in the outer region, the main deviations between μHW measurements (NSTAP included) and DNS results are found in the near-wall region, for $U/U_\infty < 0.4$, which approximately corresponds to $z^+ < 15$. These discrepancies suggest the presence of biases in the near-wall measurements of U or u' . Interestingly, these biases seem relatively independent of the micro-wire length, as no discernible trend is evident in Figure 11. This suggests that the observed bias may be attributed to the prongs, as the simple design of the μHW prototypes could induce a blockage effect, particularly near a wall. A similar trend is observed with the NSTAP, showing slighter but comparable near-wall intrusivity effects.

Profiles along the viscous-scaled wall-normal direction z^+ of velocity statistics estimated from measurements obtained with the different HW probes are displayed in Figure 12. Examining the profiles of mean velocity U^+ in Figure 12(a), an overall satisfactory collapse of all the data acquired with the different probes is observed. Compared to the reference HW probe, micro-wires achieve measurements much closer to the wall, reaching into the viscous sub-layer down to $z^+ = 2$ for the present flow configuration. However, for such near-wall locations, a bias arises due to heat transfer from the wire to the wall (Lange et al 1999), resulting in overestimated values of flow velocity as compared to the law of the wall. The second critical aspect of the μHW measurements, as already highlighted by the diagnostic plot in Figure 11, is the presence of another source of bias for z^+ below 20. This is evidenced by comparing μHW measurements with the composite ve-

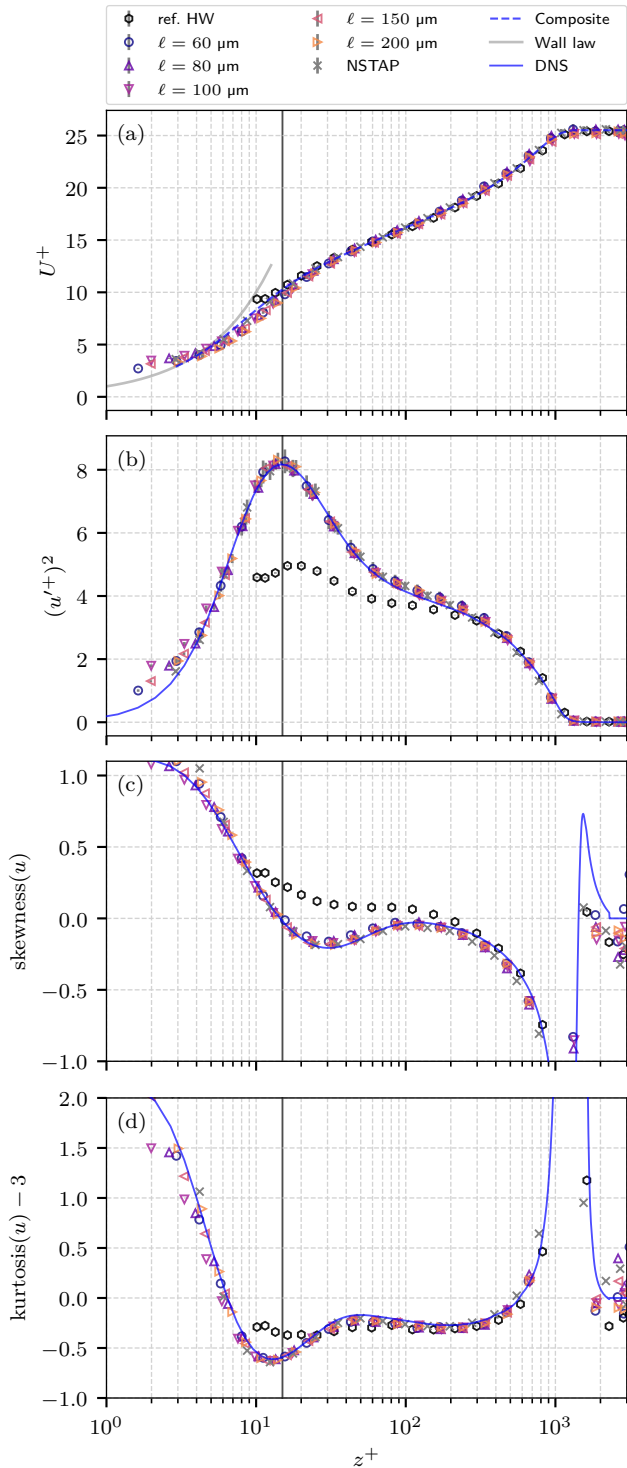


Fig. 12 Profiles of the first four moments of velocity measurements obtained with the probes listed in Table 2: (a) inner-scaled mean velocity U^+ , (b) inner-scaled velocity variance $(u'^+)^2$, (c) skewness and (d) excess kurtosis. The composite velocity profile refers to the one proposed by Chauhan et al (2007). The DNS dataset is the one used in Figure 10. Figures (a) and (b) display error-bars associated with uncertainties as evaluated in Section 4.3.

locity profile used for estimating the TBL parameters, as detailed in Section 4.3: slightly underestimated mean velocity values are observed in the buffer layer, around $z^+ \approx 10$.

Examining the profiles of viscous-scaled variance $(u'^+)^2$, skewness and excess kurtosis in Figures 12(b-d), respectively, reveals more satisfactory results, as emphasized by comparison with the DNS data of Schlatter and Örlü (2010). Notably, all the μ HW probes, including the NSTAP, yield overlapping profiles for the three moments. Classical near-wall features are well retrieved: the peak of variance and a zero-crossing of the skewness are observed at $z^+ = 15$, and the excess kurtosis reaches its minimum slightly closer to the wall. These excellent agreements thus indicate that the previously identified near-wall intrusivity effects mainly influence the mean values of local velocity distributions rather than their shapes. Finally, as expected, the reference probe, having a wire length $\ell^+ = 81$, shows inaccurate profiles mainly due to spatial filtering of near-wall small-scale structures.

5.2 Turbulent spectra

The velocity statistics obtained from the tested μ HW probes indicate no major differences, suggesting minimal spatial filtering or end-conduction effects. While limited spatial filtering was anticipated since the micro-wires meet the criterion $\ell^+ < 13$, the absence of end-conduction effects is less expected based on the analysis conducted in Section 2.4.

A finer investigation is conducted by examining viscous-scaled pre-multiplied wavenumber spectra in Figure 13 at the two wall-normal locations $z^+ \approx 15$ and $z^+ \approx 300$. Remarkably, consistent results are observed across all the μ HW probes in both cases. Even for viscous-scaled wavenumbers k_x^+ exceeding 3×10^{-2} , roughly corresponding to a frequency of 3 kHz under the current flow conditions, no significant differences are apparent. In comparison, the reference HW probe clearly yields attenuated spectra over the entire range of displayed wavenumbers in Figure 13(a) and for $k_x^+ > 3 \times 10^{-3}$ in Figure 13(b).

Referring to the frequency cut-off and attenuation predicted by the model of μ HW probes and illustrated in Figure 3, these results suggest two potential scenarios: either the frequency cut-off of the current μ HW probes is higher than anticipated, or attenuation effects are less severe than estimated. It is plausible that the model, as described in Section 2, is overly conservative, owing to approximations made in estimating the dynamic response of μ HW probes, and possibly due to uncertainties in the actual parameters of the model (such

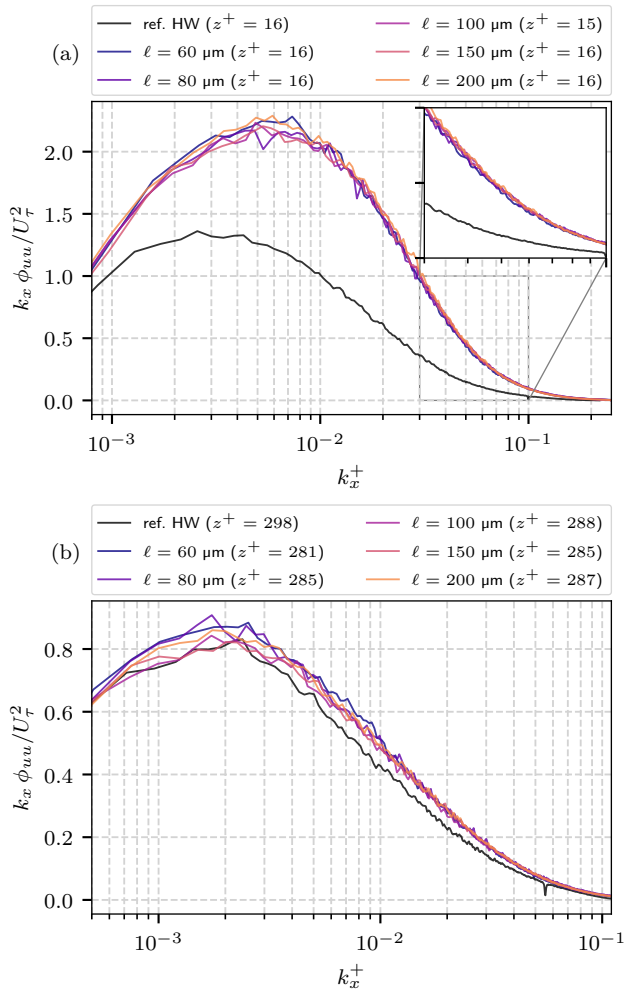


Fig. 13 Viscous-scaled pre-multiplied velocity spectra obtained with the reference HW and the μ HW probes listed in Table 2, at the wall-normal locations (a) $z^+ \approx 15$ and (b) $z^+ \approx 300$.

as material thicknesses, thermal and electrical properties of thin layers, etc.).

6 Conclusion

The concept of micro-hot-wire probes, designed with thin elongated stubs to mitigate intrusivity and spectral attenuation, was evaluated through both of an analytical 1D model and measurements in a zero-pressure-gradient TBL.

The model highlighted the effects of this design choice on both the static temperature distribution within the micro-wire and its frequency response. Overall, compared to a micro-probe without stubs, an increase of the wire extended Biot number, noted Y_w in this work, appears achievable. As a result, notable reduction in spectral attenuation can be expected. While

the developed model effectively captured the associated trends and orders of magnitude, therefore providing guidance for designing new μ HW probes and exploring the parameter space, experimental results obtained in the TBL suggest either that the model may need refinement to yield more accurate estimates of the wire frequency response, or that the model parameters are not known with sufficient accuracy. With the current model, the micro-wire spectral responses appear to be underestimated. To address these two points, dedicated studies may be considered. First, similar to Hutchins et al (2015), application to higher Reynolds-number flows should provide broadened turbulence spectra, allowing for a better identification of attenuation profiles and cut-off frequencies of the μ HW probes. Second, it is known that electrical and thermal properties of thin layers can differ from bulk values (see for example Zhang et al (2005)). A finer characterization of the Pt and SiN_x layers used in this work should thus be considered.

The experimental part of this work demonstrated the ability of these “easy-to-fabricate” prototypes of μ HW probes to provide satisfactory measurements of various moments of velocity in a ZPG TBL. Notably, the measured velocity statistics compared favorably with those obtained using the NSTAP, and these new μ HWs showed remarkable stability in thermo-resistive properties. As expected, no significant spatial filtering was observed in the results obtained with probes featuring different micro-wire lengths, all satisfying $\ell^+ < 13$. This suggests that the effective sensing part of the probe is primarily defined by the micro-wire itself, with a contribution of heated parts of the elongated stubs likely negligible. Furthermore, no discernible end-conduction effects were observed under the present flow configuration. This could be attributed to the fact that the frequency cut-offs of the μ HW probes exceed the maximum relevant frequency of the flow, calling for measurements in different flow conditions. Nonetheless, despite the use of elongated stubs likely contributing to the satisfactory measurements obtained, intrusivity effects were still identified, particularly on mean velocity profiles and in close proximity to the wall. The origin of these biases was attributed to the geometry of the prongs, suggesting that the stubs alone cannot fully address this inherent issue in HWA, necessitating further investigation into prong design. It is expected, for instance, that stationary simulations can help reproduce such intrusivity effects and thus offer insights toward improved designs for improved near-wall measurements.

Acknowledgments

The authors acknowledge the support of the staff at the Centrale de Technologie en Micro et Nanoélectronique (CTM), Université of Montpellier, France, during the micro-fabrication process. They also particularly thank Pr. M. Hultmark and A. Piqué for providing the NSTAPs used in this study.

Declarations

Ethical Approval

Not applicable.

Funding

The PhD work of B.B. was funded by the Région Occitanie, France, and ONERA.

Availability of data and materials

The data that support the findings of this study are available from the corresponding author upon reasonable request.

Open Access

For the purpose of Open Access, a CC-BY public copyright license has been applied by the authors to the present document and will be applied to all subsequent versions up to the author-accepted manuscript arising from this submission.

References

- Bailey SCC, Kunkel GJ, Hultmark M, Vallikivi M, Hill JP, Meyer KA, Tsay C, Arnold CB, Smits AJ (2010) Turbulence measurements using a nanoscale thermal anemometry probe. *Journal of Fluid Mechanics* 663:160–179, doi:[10.1017/s0022112010003447](https://doi.org/10.1017/s0022112010003447)
- Bruun HH (1996) Hot-wire anemometry: principles and signal analysis. *Measurement Science and Technology* 7(10):024
- Chauhan K, Nagib H, Monkewitz P (2007) On the Composite Logarithmic Profile in Zero Pressure Gradient Turbulent Boundary Layers. In: 45th AIAA Aerospace Sciences Meeting and Exhibit, American Institute of Aeronautics and Astronautics, Reno, Nevada, doi:[10.2514/6.2007-532](https://doi.org/10.2514/6.2007-532)
- Comte-Bellot G, Strohl A, Alcaraz E (1971) On aerodynamic disturbances caused by single hot-wire probes. *Journal of Applied Mechanics* 38(4):767–774, doi:[10.1115/1.3408953](https://doi.org/10.1115/1.3408953)
- Fan Y, Arwatz G, Buren TWV, Hoffman DE, Hultmark M (2015) Nanoscale sensing devices for turbulence measurements. *Experiments in Fluids* 56(7), doi:[10.1007/s00348-015-2000-0](https://doi.org/10.1007/s00348-015-2000-0)
- Freytmuth P (1977) Frequency response and electronic testing for constant-temperature hot-wire anemometers. *Journal of Physics E: Scientific Instruments* 10(7):705–710, doi:[10.1088/0022-3735/10/7/012](https://doi.org/10.1088/0022-3735/10/7/012)
- Freytmuth P (1979) Engineering estimate of heat conduction loss in constant temperature thermal sensors. *TSI Quart* 4:3–6
- Fu MK, Fan Y, Hultmark M (2019) Design and validation of a nanoscale cross-wire probe (x-NSTAP). *Experiments in Fluids* 60(6), doi:[10.1007/s00348-019-2743-0](https://doi.org/10.1007/s00348-019-2743-0)
- Hultmark M, Ashok A, Smits AJ (2011) A new criterion for end-conduction effects in hot-wire anemometry. *Measurement Science and Technology* 22(5):055401, doi:[10.1088/0957-0233/22/5/055401](https://doi.org/10.1088/0957-0233/22/5/055401)
- Hutchins N, Nickels TB, Marusic I, Chong MS (2009) Hot-wire spatial resolution issues in wall-bounded turbulence. *Journal of Fluid Mechanics* 635:103–136, doi:[10.1017/S0022112009007721](https://doi.org/10.1017/S0022112009007721)
- Hutchins N, Monty JP, Hultmark M, Smits AJ (2015) A direct measure of the frequency response of hot-wire anemometers: temporal resolution issues in wall-bounded turbulence. *Experiments in Fluids* 56(1), doi:[10.1007/s00348-014-1856-8](https://doi.org/10.1007/s00348-014-1856-8)
- Jiang F, Tai YC, Ho CM, Li WJ (1994) A micromachined polysilicon hot-wire anemometer. In: *Solid-State Sensor and Actuator Workshop*, pp 264–267
- Johnson RG, Holmen JO, Foster RB, Sridhar U (1990) Adhesion layer for platinum based sensors. US Patent 4,952,904
- Khoo BC, Chew YT, Teo CJ, Lim CP (1999) The dynamic response of a hot-wire anemometer: III. voltage-perturbation versus velocity-perturbation testing for near-wall hot-wire/film probes. *Measurement Science and Technology* 10(3):152–169, doi:[10.1088/0957-0233/10/3/009](https://doi.org/10.1088/0957-0233/10/3/009)
- Kokmanian K, Scharnowski S, Bross M, Duvvuri S, Fu MK, Kähler CJ, Hultmark M (2019) Development of a nanoscale hot-wire probe for supersonic flow applications. *Experiments in Fluids* 60(10), doi:[10.1007/s00348-019-2797-z](https://doi.org/10.1007/s00348-019-2797-z)
- Kunkel G, Arnold C, Smits A (2006) Development of nstap: nanoscale thermal anemometry probe. In: 36th AIAA Fluid Dynamics Conference and Exhibit, p 3718
- Lange CF, Durst F, Breuer M (1999) Correction of hot-wire measurements in the near-wall region. *Experiments in Fluids* 26(5):475–477, doi:[10.1007/s003480050312](https://doi.org/10.1007/s003480050312)
- Le-The H, Küchler C, van den Berg A, Bodenschatz E, Lohse D, Krug D (2021) Fabrication of freestanding Pt nanowires for use as thermal anemometry probes in turbulence measurements. *Microsystems & Nanoengineering* 7(1):28, doi:[10.1038/s41378-021-00255-0](https://doi.org/10.1038/s41378-021-00255-0)
- Li JD (2004) Dynamic response of constant temperature hot-wire system in turbulence velocity measurements. *Measurement Science and Technology* 15(9):1835–1847, doi:[10.1088/0957-0233/15/9/022](https://doi.org/10.1088/0957-0233/15/9/022)
- Li JD, McKeon BJ, Jiang W, Morrison JF, Smits AJ (2004) The response of hot wires in high reynolds-number turbulent pipe flow. *Measurement Science and Technology* 15(5):789–798, doi:[10.1088/0957-0233/15/5/003](https://doi.org/10.1088/0957-0233/15/5/003)
- Ligrani PM, Bradshaw P (1987a) Spatial resolution and measurement of turbulence in the viscous sublayer using subminiature hot-wire probes. *Experiments in Fluids* 5(6):407–417, doi:[10.1007/BF00264405](https://doi.org/10.1007/BF00264405)
- Ligrani PM, Bradshaw P (1987b) Subminiature hot-wire sensors: development and use. *Journal of Physics E:*

- Scientific Instruments 20(3):323–332, doi:[10.1088/0022-3735/20/3/019](https://doi.org/10.1088/0022-3735/20/3/019)
- Löfdahl L, Stemme G, Johansson B (1989) A sensor based on silicon technology for turbulence measurements. *Journal of Physics E: Scientific Instruments* 22(6):391–393, doi:[10.1088/0022-3735/22/6/013](https://doi.org/10.1088/0022-3735/22/6/013)
- Löfdahl L, Stemme G, Johansson B (1992) Silicon based flow sensors used for mean velocity and turbulence measurements. *Experiments in Fluids* 12-12(4-5):270–276, doi:[10.1007/bf00187305](https://doi.org/10.1007/bf00187305)
- Löfdahl L, Chernoray V, Haasl S, Stemme G, Sen M (2003) Characteristics of a hot-wire microsensor for time-dependent wall shear stress measurements. *Experiments in Fluids* 35(3):240–251, doi:[10.1007/s00348-003-0624-y](https://doi.org/10.1007/s00348-003-0624-y)
- McKeon B, Comte-Bellot G, Foss J, Westerweel J, Scarano F, Tropea C, Meyers J, Lee J, Cavone A, Schodl R, Koochesfahani M, Andreopoulos Y, Dahm W, Mullin J, Wallace J, Vukoslavčević P, Morris S, Pardyjak E, Cuerva A (2007) Velocity, vorticity, and mach number. In: *Springer Handbook of Experimental Fluid Mechanics*, Springer Berlin Heidelberg, pp 215–471, doi:[10.1007/978-3-540-30299-5_5](https://doi.org/10.1007/978-3-540-30299-5_5)
- Monkewitz PA (2021) Asymptotics of streamwise reynolds stress in wall turbulence. *Journal of Fluid Mechanics* 931, doi:[10.1017/jfm.2021.924](https://doi.org/10.1017/jfm.2021.924)
- Morris SC, Foss JF (2003) Transient thermal response of a hot-wire anemometer. *Measurement Science and Technology* 14(3):251–259, doi:[10.1088/0957-0233/14/3/302](https://doi.org/10.1088/0957-0233/14/3/302)
- Nagib HM, Chauhan KA (2008) Variations of von kármán coefficient in canonical flows. *Physics of Fluids* 20(10), doi:[10.1063/1.3006423](https://doi.org/10.1063/1.3006423)
- Örlü R, Fransson JH, Henrik Alfredsson P (2010) On near wall measurements of wall bounded flows—the necessity of an accurate determination of the wall position. *Progress in Aerospace Sciences* 46(8):353–387, doi:[10.1016/j.paerosci.2010.04.002](https://doi.org/10.1016/j.paerosci.2010.04.002)
- Rezaeiravesh S, Vinuesa R, Liefvendahl M, Schlatter P (2018) Assessment of uncertainties in hot-wire anemometry and oil-film interferometry measurements for wall-bounded turbulent flows. *European Journal of Mechanics - B/Fluids* 72:57–73, doi:[10.1016/j.euromechflu.2018.04.012](https://doi.org/10.1016/j.euromechflu.2018.04.012)
- Samie M, Hutchins N, Marusic I (2018a) Revisiting end conduction effects in constant temperature hot-wire anemometry. *Experiments in Fluids* 59(9):133, doi:[10.1007/s00348-018-2587-z](https://doi.org/10.1007/s00348-018-2587-z)
- Samie M, Marusic I, Hutchins N, Fu MK, Fan Y, Hultmark M, Smits AJ (2018b) Fully resolved measurements of turbulent boundary layer flows up to. *Journal of Fluid Mechanics* 851:391–415, doi:[10.1017/jfm.2018.508](https://doi.org/10.1017/jfm.2018.508)
- Sanmiguel Vila C, Vinuesa R, Discetti S, Ianiro A, Schlatter P, Örlü R (2017) On the identification of well-behaved turbulent boundary layers. *Journal of Fluid Mechanics* 822:109–138, doi:[10.1017/jfm.2017.258](https://doi.org/10.1017/jfm.2017.258)
- Schlatter P, Örlü R (2010) Assessment of direct numerical simulation data of turbulent boundary layers. *Journal of Fluid Mechanics* 659:116–126, doi:[10.1017/S0022112010003113](https://doi.org/10.1017/S0022112010003113)
- Smits AJ (2022) Batchelor prize lecture: Measurements in wall-bounded turbulence. *Journal of Fluid Mechanics* 940, doi:[10.1017/jfm.2022.83](https://doi.org/10.1017/jfm.2022.83)
- Temple-Boyer P, Rossi C, Saint-Etienne E, Scheid E (1998) Residual stress in low pressure chemical vapor deposition SiNx films deposited from silane and ammonia. *Journal of Vacuum Science & Technology A: Vacuum, Surfaces, and Films* 16(4):2003–2007, doi:[10.1116/1.581302](https://doi.org/10.1116/1.581302)
- Vallikivi M (2014) Wall-bounded turbulence at high reynolds numbers. PhD thesis, Princeton University
- Vallikivi M, Smits AJ (2014) Fabrication and Characterization of a Novel Nanoscale Thermal Anemometry Probe. *Journal of Microelectromechanical Systems* 23(4):899–907, doi:[10.1109/JMEMS.2014.2299276](https://doi.org/10.1109/JMEMS.2014.2299276)
- Vallikivi M, Hultmark M, Bailey SCC, Smits AJ (2011) Turbulence measurements in pipe flow using a nano-scale thermal anemometry probe. *Experiments in Fluids* 51(6):1521–1527, doi:[10.1007/s00348-011-1165-4](https://doi.org/10.1007/s00348-011-1165-4)
- Vallikivi M, Hultmark M, Smits AJ (2015) Turbulent boundary layer statistics at very high reynolds number. *Journal of Fluid Mechanics* 779:371–389, doi:[10.1017/jfm.2015.273](https://doi.org/10.1017/jfm.2015.273)
- Weiss J, Jondeau E, Giani A, Charlot B, Combette P (2017) Static and dynamic calibration of a MEMS calorimetric shear-stress sensor. *Sensors and Actuators A: Physical* 265:211–216, doi:[10.1016/j.sna.2017.08.048](https://doi.org/10.1016/j.sna.2017.08.048)
- Willmarth WW, Sharma LK (1984) Study of turbulent structure with hot wires smaller than the viscous length. *Journal of Fluid Mechanics* 142:121–149, doi:[10.1017/s0022112084001026](https://doi.org/10.1017/s0022112084001026)
- Zhang X, Xie H, Fujii M, Ago H, Takahashi K, Ikuta T, Abe H, Shimizu T (2005) Thermal and electrical conductivity of a suspended platinum nanofilm. *Applied Physics Letters* 86(17), doi:[10.1063/1.1921350](https://doi.org/10.1063/1.1921350)